

Prompt-In-Prompt Learning for Universal Image Restoration

Zilong Li¹ Yiming Lei¹ Chenglong Ma² Junping Zhang¹ Hongming Shan^{2,3*}

¹ Shanghai Key Lab of Intelligent Information Processing, School of Computer Science, Fudan University, Shanghai 200433, China

² Institute of Science and Technology for Brain-inspired Intelligence and MOE Frontiers Center for Brain Science, Fudan University, Shanghai 200433, China

³ Shanghai Center for Brain Science and Brain-inspired Technology, Shanghai 200031, China

{zilongli23, clma22}@m.fudan.edu.cn, {ymlei, jpzhang, hmshan}@fudan.edu.cn

Abstract

Image restoration, which aims to retrieve and enhance degraded images, is fundamental across a wide range of applications. While conventional deep learning approaches have notably improved the image quality across various tasks, they still suffer from (i) the high storage cost needed for various task-specific models and (ii) the lack of interactivity and flexibility, hindering their wider application. Drawing inspiration from the pronounced success of prompts in both linguistic and visual domains, we propose novel Prompt-In-Prompt learning for universal image restoration, named PIP. First, we present two novel prompts, a degradation-aware prompt to encode high-level degradation knowledge and a basic restoration prompt to provide essential low-level information. Second, we devise a novel prompt-to-prompt interaction module to fuse these two prompts into a universal restoration prompt. Third, we introduce a selective prompt-to-feature interaction module to modulate the degradation-related feature. By doing so, the resultant PIP works as a plug-and-play module to enhance existing restoration models for universal image restoration. Extensive experimental results demonstrate the superior performance of PIP on multiple restoration tasks, including image denoising, deraining, dehazing, deblurring, and low-light enhancement. Remarkably, PIP is interpretable, flexible, efficient, and easy-to-use, showing promising potential for real-world applications. The code is available at https://github.com/longzilicart/pip_universal.

1. Introduction

Image restoration aims to faithfully restore the high-quality clean image from various degradations (e.g., noise, rain drops, haze) encountered during image acquisition [4, 18,

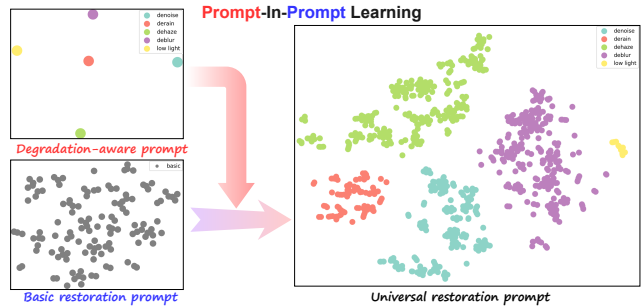


Figure 1. *t*-SNE of the proposed prompt. Prompt-in-prompt learning combines degradation-aware and basic restoration prompts for high- and low-level knowledge simultaneously. The resulting universal restoration prompt is interpretable, offering decoupled properties for different degradation types while being effective for restoration models.

44]. Due to the illness nature of the restoration task, a degraded image can be explained by multiple plausible “clean solutions” [27, 55]. Consequently, restoration poses significant challenges. Various deep learning methods have been developed [32, 69] and shown effectiveness in specific restoration tasks. However, in practical scenarios, degradation often manifests in complex forms, and may involve various degradation types (e.g., noise and rain) simultaneously. Directly applying task-specific models leads to high storage costs, limited flexibility and generalizability, thereby underscoring the need of universal restoration models.

Recently, research is shifting towards addressing multiple degradations with a single model. A straightforward approach is to modulate the parameter space for each degradation type. This includes designing additional restoration heads for different tasks [6], integrating degradation-specific paths or modules using contrastive learning [12, 29], and fine-tuning degradation-specific parameters identified by explanation methods such as integrated gradients [43, 62]. Although these approaches enhance model

adaptability to a broader range of scenarios, they still require task-specific training and additional parameters, and may fall short in offering a comprehensive solution. Prompt learning, on the other hand, enhances the input data with specific “conditions”, demonstrating impressive flexibility across different domains, and is widely used in large language models and conditional image generation. Pioneering studies like ProRes [37] and PromptIR [45] have explored using prompts to adopt models for various degradation tasks, revealing the potential of prompt learning in the field of universal image restoration.

Motivation. By reviewing the design philosophy and rationale behind the success of prompts, we find that by manipulating the input data, prompts enable a single model to effectively navigate and utilize its extensive parameter space to meet the needs of different tasks. In essence, prompts affect the input to align with the model’s trained knowledge base. When focusing on restoration tasks, prompts should assist the model in at least three key aspects. *First*, prompts should clearly identify and illustrate the overall state of degradation and navigate the model at a high level. *Second*, it should also highlight the low-level details that are relevant to the specific type of degradation and facilitate the restoration model in addressing such degradation. *Third*, prompts should modulate the feature effectively and appropriately to yield optimal results for a specific task.

Prompt-in-prompt learning. The underlying principle of prompt inspires us to design prompt-in-prompt (PIP) learning. Specifically, PIP learns two types of prompts to generate the final universal restoration prompts, as illustrated in Fig. 1. Imitating the decoupled nature of human language, PIP first learns well-defined degradation-aware prompt to represent specific degradation types and concepts, which serve as a high-level condition to modify the input. Nonetheless, degradation-aware prompt may not be sufficient to guide the restoration process directly [37], while the degradation patterns are hard to describe via simple words or conditions and require detailed and textured representations. Hence, we propose to learn a basic restoration prompt for key low-level features of various degradations, including essential textures and fine structures, which are more compatible with restoration models. Given these two types of prompts, we then design a novel *prompt-to-prompt (P2P) interaction* module to fuse them to generate the final universal restoration prompt, which encodes both rich semantics of degradation and essential detailed information for restoration. Unlike linguistic prompts with distinct word meanings, restoration prompts often contain extraneous information, reflecting the complexity of image degradation. For example, rain within an image may exhibit different directional shifts (left or right), posing challenges in formulating precise prompts. Hence, instead of directly utilizing the generated prompts to interact with the features,

we further introduce *selective prompt-to-feature (P2F) interaction* to focus only on the most effective features denoted by the attention map.

With the core design mentioned above, PIP works as a plug-and-play module to enhance existing single-task models for universal restoration. While PIP can be integrated into various positions of a network, we propose to apply it exclusively to the skip connections of the prevalent U-shape networks in the field of image restoration. This is because the skip connections contribute mainly to those high-frequency details that differ significantly among tasks, where PIP can better unlock its potential without much computational cost.

Contributions. Our contributions are as follows.

- We propose prompt-in-prompt learning for universal image restoration, which involves learning high-level degradation-aware prompts and low-level basic restoration prompts simultaneously.
- We devise a prompt-to-prompt interaction module to fuse these two prompts for a universal restoration prompt.
- We introduce a selective prompt-to-feature interaction module to modulate the most degradation-related features for a specific restoration task.
- Extensive experimental results across various restoration tasks demonstrate the superior performance of our PIP. We also highlight that PIP is interpretable, flexible, efficient, and easy to use.

2. Related work

Multi-task restoration network. Image restoration aims to recover clean images or signals from their degraded version, which is significantly different for each task. To this end, the literature proposes various methods for an individual degradation task by fully considering the degradation prior [7, 13–15, 30, 30, 32, 51, 51, 54, 68, 69]. Compared with single-task restoration, multi-task restoration is more applicable and advantageous in model storage efficiency. The primary challenge lies in using a single model to handle various types of degradation and accordingly restore the specific components. One solution is to modify the parameter space to fit the model for different degradations [29, 43, 61]. For example, IPT [6] proposes to utilize a pre-trained transformer backbone with different encoders and decoder heads to restore various degradation images. DASR [61] and AirNet [29] propose to learn discriminative degradation representation, which is then used to guide the restoration process. ADMS [43] proposes to utilize filter attribution integral gradient (FAIG) [62] to find the most discriminative parameters related to different components to learn another set of these parameters to better fit different tasks. Given the complexity of degradation, these approaches lack flexibility and can still incur considerable storage costs.

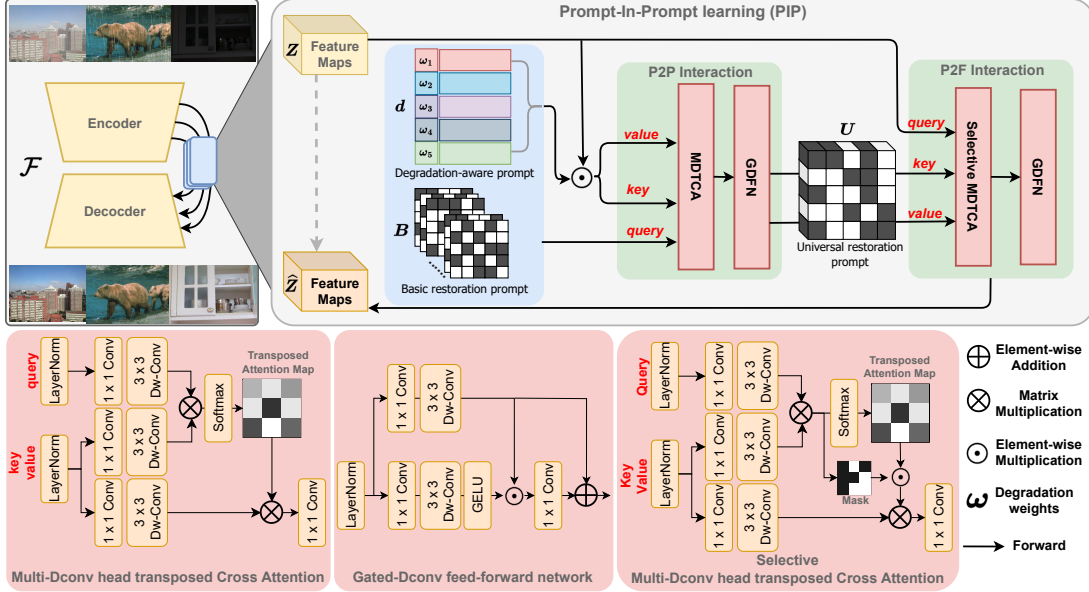


Figure 2. The architecture of PIP, which is developed as a lightweight, plug-and-play module on the skip connection to enhance current task-specific networks for universal restoration. PIP first learns degradation-aware prompt d and basic restoration prompt B , and then generates the universal restoration prompt U by prompt-to-prompt (P2P) interaction. Lastly, features Z are modulated via selective prompt-to-feature (P2F) interaction, focusing on the most relevant features denoted by the prompt.

Prompt, on the other hand, can be considered as a well-known prior recognized by the model and thus conditioning inputs for ideal outputs. Motivated by its easy implementation and high generalization, pioneering studies like ProRes [37] and PromptIR [45] have utilized prompts to extend models to various degradations. Specifically, ProRes proposes adding a learnable prompt in the input image, while PromptIR uses various prompts to modulate the feature map. Although they have demonstrated potential in enhancing restoration performance with prompts, there remains a substantial disparity between the performance and the controllability exhibited by prompts in other tasks, such as image generation and editing [47, 60, 63]. *This paper develops a lightweight plug-and-play module named PIP, which enhances existing backbones for state-of-the-art performance in universal restoration while providing flexible interaction and interpretability.* Please refer to Sec. A in Supplementary Material for detailed related work.

Prompt learning in vision. Prompt learning has emerged as a pivotal technique in the field of large language models (LLMs) [35, 66]. Research indicates that incorporating prompts into the input can significantly enhance model performance, offering exciting zero-shot or few-shot ability. The primary benefit of using prompts lies in their simplicity and flexibility. By merely “prompting” the model with some additional inputs, LLMs can be effectively adapted to a wide range of tasks and scenarios, which is particularly valuable in practical applications [60, 72]. Vision prompts

have also shown promise across multiple tasks, particularly in AIGC tasks such as image generation, inpainting, and editing. Notably, studies have expanded prompts to include vision priors such as segmentation masks, points, or anchor boxes [25, 26, 50, 58, 63]. However, most of them still focus on high-level vision tasks.

By reviewing the philosophy of prompt learning from an image restoration perspective, this paper proposes *prompt-in-prompt learning*, which simultaneously learns high-level degradation-aware knowledge and essential low-level information to prompt existing restoration models. Notably, our design may also benefit other low-level tasks with prompts.

3. Method

3.1. Problem Definition

Image restoration aims to reconstruct a clean image Y , from its degraded counterpart X , represented as $X = \mathcal{D}(Y)$, where \mathcal{D} denotes the degradation process such as noise, rain, haze, *etc.* Given a degraded image, conventional approaches employ separate task-specific model $\mathcal{F}_{\mathcal{D}}$ for each degradation \mathcal{D} :

$$\hat{Y} = \mathcal{F}_{\mathcal{D}}(X), \quad (1)$$

where \hat{Y} is the restored image. In the real restoration scenarios, different degraded images may exhibit, *e.g.*, X_{noise} , X_{rain} , and X_{haze} . Simply implementing task-specific models is unsuitable, resulting in high storage costs and limited

flexibility. Recognizing the intricacies of practical scenarios, the demand for a universal restoration model \mathcal{F} has surged, which aims at tackling different degradations and consistently generating high-quality restored outputs:

$$\hat{Y} = \mathcal{F}(X). \quad (2)$$

3.2. Overview of PIP

Fig. 2 presents the overview of our PIP, which works as a plug-and-play module applied to the skip-connections of a U-shape encoder-decoder network. The key components in PIP are two prompts: the degradation-aware prompt to encode high-level degradation knowledge and the basic restoration prompt to provide essential low-level information. These two prompts are then fused to produce the universal restoration prompt through a prompt-to-prompt interaction module, which is used to further modulate the most degradation-related features through a selective prompt-to-feature interaction module.

Concretely, PIP modulates the network \mathcal{F} on latent features Z for different degradations with degradation weights ω . The modulated features \hat{Z} is given by:

$$\hat{Z} = \text{PIP}(Z, \omega), \quad (3)$$

where $\omega = [\omega_1, \omega_2, \dots, \omega_T]$ denotes the degradation-specific weights and T is the number of degradation types. Notably, we keep ω as the unique controllable interface of PIP to provide flexible interaction by either human or degradation-assessment models.

In the following, we details these two prompts in PIP. **Degradation-aware prompt.** In the realm of the large language models, the prompt is known for its remarkable flexibility and controllability, which facilitates user interaction and provides meaningful interpretability [60, 72]. In low-level vision, however, describing the degradation with a few words is difficult due to the complexity of degradation. Finding an effective way to incorporate the degradation concept into models remains challenging. One essential design of PIP is to learn a group of decoupled, degradation-aware prompts during training. These prompts are learned to clearly represent the concepts of different degradation types, akin to the clarity of human languages. This provides clear interpretation and enables seamless interaction and control by humans and degradation-aware models.

Specifically, we use a 1D vector d_t to denote the degradation-aware prompt for t -th degradation type, and all prompts, $\{d_t\}_{t=1}^T$, should be directionally decoupled. To achieve this, we conduct a directional decoupled loss among them, which is defined as:

$$\mathcal{L}_{\text{ddl}} = \frac{2}{T(T-1)} \sum_{i=1}^{T-1} \sum_{j=i+1}^T \max(0, \theta_{\text{thre}} - \theta_{ij}),$$

$$\text{where } \theta_{ij} = \cos^{-1} \left(\frac{d_i^T d_j}{\max(\|d_i\|_2 \|d_j\|_2, \epsilon)} \right), \quad (4)$$

where the loss \mathcal{L}_{ddl} computes the sum of the differences between a threshold angle θ_{thre} and angle θ_{ij} across all pairs. ϵ is set as 1×10^{-8} to avoid division by zero. This encourages the angles between degradation-aware prompts to be at least θ_{thre} degrees.

Since the degradation types are easy to obtain during training, well-decoupled degradation-aware prompts can be easily learned under supervision. Unlike previous prompt learning that has no explicit learning target [37, 45], ours can provide rich knowledge and semantic information of the degradation type through Eq. (4), thereby offering richer interpretability and flexibility.

Basic restoration prompt. Although we have degradation-aware prompts denoting the degradation types, it still requires detailed and low-level feature representations for the restoration models. Hence, we propose to learn a task-unrelated basic restoration prompt for key low-level features among various degradations, including essential textures and fine structures. The basic restoration prompt is denoted as $B \in \mathbb{R}^{c \times h \times w}$, where c , h , and w denote the channel, height, and width of the prompt, respectively. Compared with d , B may not be easily understood or controlled by humans but is more compatible with restoration models.

Next, we detail how to fuse these two prompts and modulate the features, followed by the training and optimization of PIP.

3.3. Prompt-to-Prompt Interaction

The magic of prompts in vision-language models can be largely attributed to the pre-trained vision-language models such as CLIP [46] and BLIP [31], which link concepts across different modalities in a shared space.

For image restoration, fusing the degradation-aware prompt d and basic restoration prompt B is also important. Therefore, we design a prompt-to-prompt interaction module, using d as prompts to guide the generation of the final universal restoration prompt from B . Specifically, we multiply degradation-aware prompt d with the weights ω , and then perform element-wise multiplication with the output and Z along the channel dimension. Then, the output is reshaped and repeated on the width and height to the same shape of the basic restoration prompt B to obtain \hat{D} . Finally, these two prompts are fused via cross attention mechanism [5, 23, 47], which is defined as:

$$\text{CAtt}(\mathbf{Q}_b, \mathbf{K}_d, \mathbf{V}_d) = \text{softmax} \left(\mathbf{Q}_b \mathbf{K}_d^T / \sqrt{d_k} \right) \mathbf{V}_d, \quad (5)$$

where the query \mathbf{Q}_b is derived from the basic restoration prompt B , and the key \mathbf{K}_d and value \mathbf{V}_d are derived from \hat{D} ; in detail, these three matrices are generated through layer normalization, 1×1 convolutions, and 3×3 depth-wise convolutions as orders, as illustrated in Fig. 2. Since conventional attention mechanism with learnable matrices [56]

can introduce extremely high computation costs and can not well-fit features of different shapes, which are commonly met in image restoration, we adopted the design of Multi-Dconv head Transposed Attention (MDTA) [69] to build our cross attention. Then, we employ Gated-Dconv Feed-forward Network (GDFN) [69] to generate the universal restoration prompt U for feature modulation based on the attention map and B . The prompt-to-prompt interaction can be written as:

$$U = \text{GDFN}(B + \text{CAtt}(\mathbf{Q}_b, \mathbf{K}_d, \mathbf{V}_d)). \quad (6)$$

Finally, the resulting universal restoration prompt U serves as the prompt of features with both knowledge of degradation type and can be well understood by restoration models.

3.4. Prompt-To-Feature Interaction

As outlined in Sec. 2, a key challenge in image restoration lies in addressing various types of degradation with a single model, each focusing on different details. For instance, image denoising targets high-frequency details like textures while image deblurring and low-light enhancement prioritize restoring structural and global value shifts. To this end, we design prompt-to-feature interaction to modulate the most degradation-related features.

Selective prompt modulation. Although the generated universal restoration prompt U can well fit specific degradations, not all the components have an equal contribution to a specific image. Motivated by sparsity transformer [9, 13], we proposed to be more selective during prompt-to-feature interaction to focus on modulating the most degradation-related feature. Specifically, we compute the transposed cross attention map $A \in \mathbb{R}^{C \times C}$ with channel C , where each channel identifies the attention score of U and input feature Z across the channels, and each row indicates the scores of a typical channel of the feature to the total C prompts. Since each channel of feature maps carries a specific meaning of the image, we then select a partial of the attention map in each row using a mask $M \in \mathbb{R}^{C \times C}$ that denotes the most important prompt. Similar to previous work [13, 57], we select top- m values of each row by applying the mask M defined as follows:

$$M_{ij} = \begin{cases} 1, & A_{ij} \geq \text{Top}_m(A_{i.}), \\ 0, & \text{otherwise.} \end{cases} \quad (7)$$

where $\text{Top}_m(A_{i.})$ denotes the m largest values in the i -th row of A . Then, we produce element-wise multiplication on the attention map and mask to compute the cross-attention output, which can be written as:

$$\text{CAtt}_s(\mathbf{Q}_z, \mathbf{K}_u, \mathbf{V}_u) = \text{softmax} \left(M \odot \frac{\mathbf{Q}_z \mathbf{K}_u^T}{\sqrt{d_k}} \right) \mathbf{V}_u, \quad (8)$$

where the query \mathbf{Q}_z is derived from feature Z , and the key \mathbf{K}_u and value \mathbf{V}_u are derived from universal restoration prompt U . \odot represents the element-wise multiplication. Lastly, the modulated feature \hat{Z} from the original feature Z is given by:

$$\hat{Z} = \text{GDFN}(Z + \text{CAtt}_s(\mathbf{Q}_z, \mathbf{K}_u, \mathbf{V}_u)). \quad (9)$$

3.5. Training and Optimization

We train PIP on multiple datasets for universal restoration. Specifically, we integrate PIP into the skip connection of U-shape backbones, as early-stage features exhibit more significant differences between tasks. During the training phase, the degradation weights ω are given as one-hot labels to select the degradation-aware prompt. We incorporate PIP on the widely used backbones, including Restormer [69] and NAFNet [8]. To focus on the effect of PIP, we only involve the most common optimization process, with random horizontal and vertical flips as the data augmentation and pixel-wise \mathcal{L}_1 for restoration loss. The total loss of PIP can be written as:

$$\mathcal{L} = \mathcal{L}_1 + \alpha \mathcal{L}_{\text{ddl}}, \quad (10)$$

where α is a trade-off hyperparameter.

4. Result

We conduct experiments on five restoration tasks, including image denoising, deraining, dehazing, deblurring, and low-light enhancement.

4.1. Experimental Setup

Dataset. Regarding image denoising, deraining, and dehazing, we use datasets in line with previous works [29, 45]. The training datasets include BSD400 [3] and WED [38] for denoising by adding Gaussian noise levels $\sigma \in \{15, 25, 50\}$, Rain100L [64] for deraining, and SOTS [28] for dehazing. In addition, we include two challenging tasks of image deblurring and low-light enhancement and use the GoPro [41] and LOL dataset [59] for training, as previous research [8, 69, 70]. For all the datasets, we follow the standard practices in data splitting and pre-processing in the field. Finally, we train and evaluate PIP jointly on multiple datasets, using the three-task configuration “noise-rain-haze” and the five-task setup “noise-rain-haze-blur-enhance”. Please refer to Sec. B in Supplementary Material for more detailed information about the training and testing datasets.

Implementation details. During the training phase, the degradation weights ω are given as one-hot labels to select the degradation-aware prompt in a supervised fashion. We incorporate PIP on the widely used backbones, including Restormer and RAPNet on the skip connections. For

Table 1. Performance on “noise-rain-haze” settings. The best and second best results are marked in **bold** and underline, respectively.

Method	Denoise (BSD68)			Dehaze (SOTS)	Derain (Rain100L)	Average
	$\sigma = 15$	$\sigma = 25$	$\sigma = 50$			
BRDNet [52]	32.26/0.898	29.76/0.836	26.34/0.836	23.23/0.895	27.42/0.895	27.80/0.843
LPNet [21]	26.47/0.778	24.77/0.748	21.26/0.552	20.84/0.828	24.88/0.784	23.64/0.738
FDGAN [19]	30.25/0.910	28.81/0.868	26.43/0.776	24.71/0.924	29.89/0.933	28.02/0.883
MPRNet [68]	33.54/0.927	30.89/0.880	27.56/0.779	25.28/0.954	33.57/0.954	30.17/0.899
DL [20]	33.05/0.914	30.41/0.861	26.90/0.740	26.92/0.391	32.62/0.931	29.98/0.875
AirNet [29]	33.92/0.933	31.26/0.888	28.00/0.797	27.94/0.962	34.90/0.967	31.20/0.910
PromptIR [45]	<u>33.98/0.933</u>	<u>31.31/0.888</u>	<u>28.06/0.799</u>	<u>30.58/0.974</u>	<u>36.37/0.972</u>	<u>32.06/0.913</u>
PIP _{Restormer}	34.24/0.936	31.60/0.893	28.35/0.806	32.09/0.981	38.29/0.984	32.91/0.920

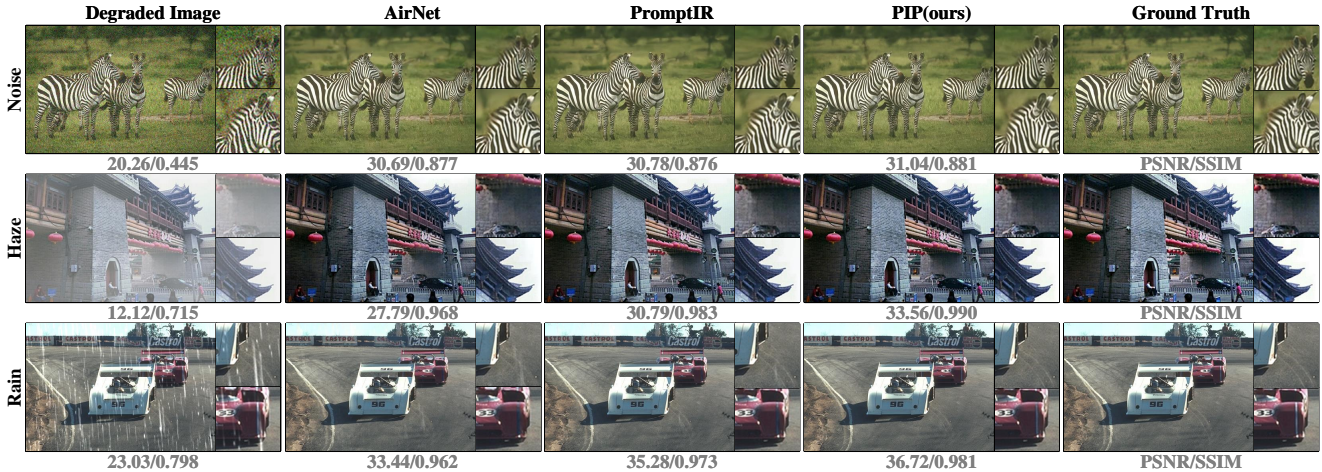


Figure 3. Visual comparison of universal methods on image denoising, deraining, and dehazing.

simplicity, we utilize Adam optimizer with $\beta_1 = 0.9$ and $\beta_2 = 0.99$ to optimize the network. The learning rate is set to 5×10^{-4} with a total batch size of 32 for 200 epochs on 8 RTX4090 GPUs. During training, we utilized cropped patches with a size of 128×128 for 150 epochs and 200×200 for the rest 50 epochs, using random horizontal and vertical flips as the only augmentation. The θ_{thre} of \mathcal{L}_{ddl} is set to 90° , and α is set to 0.002. In addition to the default settings, we have also developed a data augmentation strategy to introduce multiple degradation types for prompt learning, which is similar to CutMix [22, 67]. This is not involved by default for fair comparison. Please refer to Sec. B in Supplementary Material for more implementation details, such as the training procedure and network configuration.

Evaluation metrics and comparisons methods. We use the peak signal-to-noise ratio (PSNR) and the structural similarity (SSIM) [73] to evaluate the performance. We plug PIP on the skip connection of Restormer [69] and NAFNet [8] for PIP_{Restormer} and PIP_{NAFNet}. Regarding universal restoration methods, we mainly take the state-of-the-art AirNet [29] and PromptIR [45] for comparison by using the official checkpoint.

4.2. Performance on Image Restoration Tasks

Multi-task performance evaluation. Tab. 1 presents the overall performance of PIP and other state-of-the-art methods on “noise-rain-haze” setting. We find that our PIP outperforms the state-of-the-art PromptIR [45] with the same backbone of Restormer [69] across various tasks, demonstrating the effectiveness of our PIP. Notably, PIP demonstrates significant improvements in challenging, severe degradation tasks such as image deraining and dehazing, outperforming PromptIR by over 1.5 dB in PSNR. Fig. 3 shows the restoration results of various methods for image denoising, deraining, and dehazing. we find that PIP achieves better visual quality with less noise and artifacts than the other methods.

In addition, we find that previous methods tend to eliminate those image details similar to the degradation. For instance, in the third row of Fig. 3, both AirNet and PromptIR remove the white tire line that resembles a raindrop, while PIP successfully retains the details. This is largely due to the high-quality universal restoration prompt proposed in this paper, which effectively guides the network to accurately remove those degradation-related patterns.

Enhancing restoration backbone with PIP. We also assess the performance of PIP over a broader spectrum of

Table 2. Performance on “noise-rain-haze-blur-enhance” datasets. The best and second best results of multi-task restoration are marked in **bold** and underline, respectively. Metrics are presented in [PSNR (dB) / SSIM]. Metrics are presented in [PSNR (dB) / SSIM].

Cat.	Method	Denoise (BSD68)			Dehaze (SOTS)	Derain (Rain100L)	Deblur (GoPro)	Lowlight (LOL)	Average
		$\sigma = 15$	$\sigma = 25$	$\sigma = 50$					
Single	SwinIR [32]	34.42/-	31.78/-	28.56/-	-	-	-	-	-
	Restormer [69]	34.40/-	31.79/-	28.60/-	-	37.61/0.975	32.92/0.961	-	-
	NAFNet [8]	-	-	-	-	-	33.69/0.967	-	-
Multi.	Restormer [69]	33.55/0.926	30.96/0.879	27.75/0.784	29.50/0.973	36.53/0.974	27.31/0.835	23.00/0.841	29.94/0.887
	NAFNet [8]	33.71/0.930	31.12/0.884	27.91/0.793	30.67/0.975	37.17/0.976	28.32/0.863	23.18/0.856	30.29/0.896
	PromptIR [45]	33.67/0.929	31.08/0.883	27.87/0.787	30.16/0.977	37.16/0.977	28.73/0.868	23.91/0.848	30.36/0.895
Ours	PIP _{NAFNet}	34.10/0.935	<u>31.45/0.893</u>	28.21/0.806	<u>31.75/0.978</u>	<u>37.67/0.980</u>	28.08/0.853	23.37/0.854	<u>30.66/0.899</u>
	PIP _{Restormer}	<u>34.05/0.934</u>	31.48/0.891	<u>27.29/0.805</u>	32.11/0.979	38.09/0.983	<u>28.61/0.861</u>	24.06/0.859	30.81/0.901



Figure 4. Visualization results of using different degradation-aware prompts for restoration.

degradation types compared to baseline methods, by training and testing PIP and other comparison methods on the five-task setting. This is more challenging due to severe corruption in blurred and low-light images. Tab. 2 shows the performance of each method. We note that we adopt the results reported in the original papers for the single-task methods. Since most of them are optimized with techniques such as progressive training [69] and may be trained on different datasets, they can be regarded as the upper bound for universal models. Through comparison across multi-task methods, we find that PIP achieves superior results and effectively improves the backbone models for universal restoration. By integrating PIP into Restormer, there are noticeable performance gains by at least 0.5 dB and up to 1.5 dB in challenging tasks like deblurring and deraining, respectively. Similar observation can be found by comparing PIP_{NAFNet} and NAFNet, demonstrating the effectiveness of PIP on various backbones. As expected, PIP suffers from a performance drop in image denoising and deraining compared to results in Tab. 1, but image dehazing gets a slight improvement. This may be attributed to the limited parameter numbers for both the backbone networks and PIP. Generally, we find that PIP is able to effectively handle a broader range of degradations and maintains good perfor-

mance. In contrast, conventional prompt-based restoration methods such as PromptIR tend to suffer considerable performance drop when dealing with increasing types of degradation compared to Tab. 1.

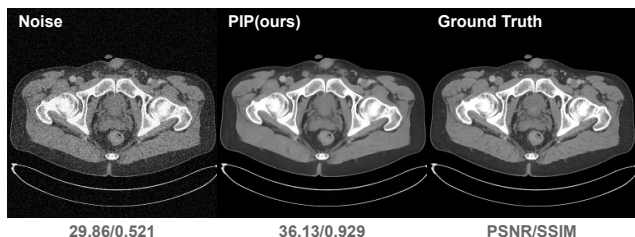


Figure 5. Visualization of PIP on CT denoising with noise level $\sigma = 25$ under a CT window of $[-200, 300]$ HU.

Performance on out-of-distribution data. We further evaluate PIP and other universal models on out-of-distribution data, as presented in Tab. 3. Generally, we find that PIP outperforms other universal methods on various out-of-distribution degradations, particularly when adapting to unseen noise levels of $\sigma \in \{10, 30, 60\}$ and heavy rain degradation on Rain100H [64]. PIP also better handles the multiple degradations than comparison methods. Additionally, we directly use PIP for CT image denoising

Table 3. Performance on unseen noise level of ($\sigma = 10, 30, 60$) and severe rain conditions from the Rain100H dataset. Additional noise ($\sigma = 25$) was added to the rain and haze test sets to generate images with multiple degradations.

Method	Denoise (Urban100)			Rain100H	Rain100L + Noise	Haze + Noise	Average
	$\sigma = 10$	$\sigma = 30$	$\sigma = 60$				
AirNet [29]	35.26/0.952	30.04/0.880	25.41/0.714	14.55/0.478	24.93/0.768	15.94/0.753	24.35/0.757
PromptIR [45]	35.77/0.958	30.66/0.901	27.03/0.817	15.54/0.486	24.92/0.767	15.93/0.752	24.97/0.780
PIP _{Restormer}	36.17/0.960	31.24/0.909	27.30/0.809	16.29/0.501	26.50/0.771	16.58/0.754	25.68/0.784

Table 4. Efficiency comparison, including number of parameters, FLOPS, and average inference time. The testing is conducted on a single RTX2080Ti GPU using 1000 images with a batch size of 1, each at a resolution of 256×256 .

Method	Param. (M)	FLOPS (G)	Infer. (ms)
AirNet [29]	5.767	301.27	417.43
Restormer [69]	26.09	140.99	225.87
PromptIR [45]	32.96 ($\uparrow 26.32\%$)	158.14 ($\uparrow 12.16\%$)	251.98 ($\uparrow 11.56\%$)
PIP _{Restormer}	26.82 ($\uparrow 2.77\%$)	154.72 ($\uparrow 9.74\%$)	245.33 ($\uparrow 8.62\%$)

and find PIP robust, as present in Fig. 5. Please refer to Sec. C in Supplementary Materials for more quantitative and qualitative results, including zero-shot performance on real-world datasets and medical images. we also discuss how to better fit PIP for multiple degradations by controlling the degradation-aware prompt and training with data augmentation.

4.3. Efficiency

Tab. 4 showcases the efficiency of various methods in terms of the number of parameters, FLOPS, and average inference time. These results are obtained on a single RTX2080Ti GPU, using a batch size of 1, and were averaged over 1000 images at a resolution of 256×256 . We observe that the proposed PIP is efficient, causing only a slight increase in parameters and FLOPS but resulting in notable performance gain when compared to the backbone. It also outperforms PromptIR, which significantly increases the number of parameters. In conclusion, PIP is lightweight, and only increases a barely amount of extra computation costs while achieving good performance.

4.4. Ablation Study

We evaluate the effectiveness of each component under “noise-rain-haze” settings, and present the average results in Tab. 5. For configurations a), b) and d) without prompt-in-prompt learning, we repeat and resize them to the same shape as the universal restoration prompt. For other configurations without selective prompt-to-feature interaction, we use the Multi-Dconv head transposed Cross Attention to replace the selective one.

Ablation on prompt-in-prompt learning. Degradation-aware prompts play a crucial role in PIP by integrating the high-level degradation information into the restoration process. By comparing configurations b) and c) in Tab. 5, we find that the degradation-aware prompts effectively en-

Table 5. Quantitative evaluation of different configurations of PIP under “noise-rain-haze” datasets. \mathbf{d} and \mathbf{B} are the degradation-aware prompt and basic restoration prompt, respectively.

Config.	\mathbf{d}	\mathbf{B}	selective P2F	Avg. PSNR/SSIM
a)	✓			31.85/0.908
b)		✓		32.07/0.911
c)	✓	✓		32.62/0.918
d)		✓	✓	32.15/0.912
e)	✓	✓	✓	32.91/0.920

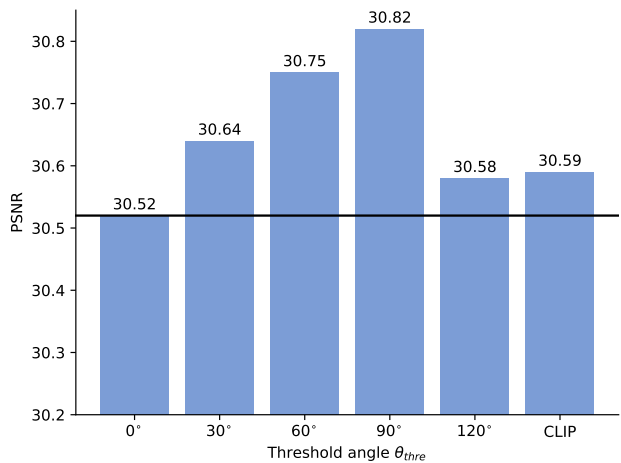


Figure 6. The effect of varying θ_{thre} in \mathcal{L}_{ddl} from 0° to 120° during training. The black horizontal line indicates \mathcal{L} with $\alpha = 0$, which imposes no constraint on the degradation-aware prompt; note that it also corresponds to $\theta_{thre} = 0^\circ$. In the “CLIP” configuration, a pre-trained CLIP text encoder [46] and a linear layer are used to create degradation-aware prompts of the same shape. The experiments are conducted on a four-dataset setting of “noise-rain-blur-enhance” to reduce the computation costs, considering the dehazing dataset is the largest one.

hance the overall performance. To further assess the effectiveness of the proposed method, we examine PIP using both accurate and inaccurate prompts. As illustrated in Fig. 4, degradation-aware prompts are highly effective and manifest a decoupled behavior, distinct for each degradation type. For instance, only images with the correct prompt, such as “derain” in the second row and “enhance” in the third row, are successfully restored, and using incorrect prompt results in notable performance drop or restoration failure. We also find that relying solely on the degradation prompts leads to sub-optimal results in a), b) and c). This can be attributed to the misalignment of high-level and low-level knowledge. These results highlight the effectiveness of the proposed prompt-in-prompt learning, and the resultant universal restoration prompt can benefit universal restoration in both high- and low-level aspects.

Ablation on selective prompt-to-feature interaction. By comparing b) and d) in Tab. 5, we find that selective prompt-to-feature interaction is beneficial for restoration. This could stem from the imprecise and abundant of restoration prompts while selective interaction can focus on the most pertinent features for a specific degradation. Upon comparing e) and c), both with prompt-in-prompt learning, selective interaction leads to more significant advancements. This is likely due to the improved quality of the universal restoration prompts, which positively guides the selection.

Ablation on \mathcal{L}_{ddl} and \mathcal{L} . We explore how different settings of the trade-off hyperparameter α in \mathcal{L} and the threshold angle θ_{thre} in \mathcal{L}_{ddl} would affect the restoration performance. Specifically, $\alpha = 0$ implies no constraints on the learnable degradation-aware prompts, whereas $\theta_{\text{thre}} = 90^\circ$ indicates that the prompts are entirely distinct. As shown in Fig. 6, settings with $\alpha = 0$ and $\theta_{\text{thre}} = 0^\circ$ are less effective compared to others. This might be due to the entanglement of different degradation-aware prompts, hindering the model from using high-level knowledge. Notably, increasing θ_{thre} improve the performance, with a notable gain of 0.3db when comparing $\theta_{\text{thre}} = 90^\circ$ to $\theta_{\text{thre}} = 0^\circ$. This suggests that decoupled degradation-aware prompts can enhance restoration. We also find that $\theta_{\text{thre}} = 120^\circ$ leads to a performance drop compared to $\theta_{\text{thre}} = 90^\circ$. In summary, we choose $\theta_{\text{thre}} = 90^\circ$ for better performance.

Additionally, we study the efficacy of using a pre-trained CLIP text-encoder [46] to generate the high-level degradation-aware prompt. Note that the CLIP text encoder also produces a 1D vector of size 512. We first use degradation classes like “noise” or “blur” to get language embeddings from CLIP and then project these embeddings through a linear layer to generate degradation-aware prompts of the same shape. We find that this approach performs better than configurations without constraints, yet it is still less optimal compared to our default

setting of $\theta_{\text{thre}} = 90^\circ$, as presented in Fig. 6.

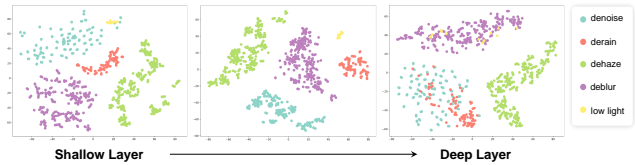


Figure 7. t -SNE visualization of the three universal restoration prompt in $\text{PIP}_{\text{Restormer}}$. Each color represents one degradation type.

5. Discussion

Interpretability. We visualize the t -SNE of the three generated universal restoration prompts for each skip-connection in Fig. 7. Interestingly, we find they are well-clustered in terms of the degradation types. In shallow layers, the universal restoration prompt is less compact to fit diverse image details compared to the middle layer. In the deep layer, on the other hand, some degradation types show correlation and cluster together. This phenomenon might occur because degradations such as rain and noise, both influenced by high-frequency noise, share similar features in deep layers. Generally, by learning clear degradation concepts, PIP is interpretable and flexible. Since PIP is designed as a plug-and-play module, it is also easy to use and can effectively enhance backbone models.

Control by degradation-aware models. PIP is designed to focus on enhancing the restoration performance rather than automatically recognizing different tasks. This is due to the complicated nature of degradation and various requirements in application. For instance, a user may want to remove noise from a low-light image without increasing brightness. However, we note that PIP can be *easily controlled via a simple degradation-aware model without performance drop*, referring to the result in Sec. C of Supplementary Materials. In general, PIP is flexible and can easily adapt to different requirements.

6. Conclusion

This paper proposes a novel prompt-in-prompt learning for universal image restoration. PIP involves learning high-level degradation-aware prompts and low-level basic restoration prompts simultaneously to produce the effective universal restoration prompt. By modulating the most degradation-related features with a selective prompt-to-feature interaction module, PIP achieves superior and robust performance on various restoration tasks. PIP is also efficient and lightweight, making it easily adaptable to diverse models and enhancing them for universal image restoration.

References

- [1] Abdelrahman Abdelhamed, Stephen Lin, and Michael S Brown. A high-quality denoising dataset for smartphone cameras. In *Proceedings of the IEEE Conference on Computer Vision and Pattern Recognition*, pages 1692–1700, 2018. 4
- [2] Cosmin Ancuti, Codruta Orniana Ancuti, Tom Haber, and Philippe Bekaert. Enhancing underwater images and videos by fusion. *2012 IEEE Conference on Computer Vision and Pattern Recognition*, pages 81–88, 2012. 1
- [3] Pablo Arbelaez, Michael Maire, Charless Fowlkes, and Jitendra Malik. Contour detection and hierarchical image segmentation. *IEEE Transactions on Pattern Analysis and Machine Intelligence*, 33(5):898–916, 2010. 5, 1, 2
- [4] Mark R Banham and Aggelos K Katsaggelos. Digital image restoration. *IEEE Signal Processing Magazine*, 14(2):24–41, 1997. 1
- [5] Chun-Fu Chen, Quanfu Fan, and Rameswar Panda. Crossvit: Cross-attention multi-scale vision transformer for image classification. *2021 IEEE/CVF International Conference on Computer Vision (ICCV)*, pages 347–356, 2021. 4
- [6] Hanting Chen, Yunhe Wang, Tianyu Guo, Chang Xu, Yiping Deng, Zhenhua Liu, Siwei Ma, Chunjing Xu, Chao Xu, and Wen Gao. Pre-trained image processing transformer. In *Proceedings of the IEEE/CVF Conference on Computer Vision and Pattern Recognition*, pages 12299–12310, 2021. 1, 2
- [7] Liangyu Chen, Xin Lu, Jie Zhang, Xiaojie Chu, and Chengpeng Chen. Hinet: Half instance normalization network for image restoration. In *Proceedings of the IEEE/CVF Conference on Computer Vision and Pattern Recognition*, pages 182–192, 2021. 2, 1
- [8] Liangyu Chen, Xiaojie Chu, Xiangyu Zhang, and Jian Sun. Simple baselines for image restoration. In *European Conference on Computer Vision*, pages 17–33. Springer, 2022. 5, 6, 7, 1
- [9] Tianlong Chen, Yu Cheng, Zhe Gan, Lu Yuan, Lei Zhang, and Zhangyang Wang. Chasing sparsity in vision transformers: An end-to-end exploration. *Advances in Neural Information Processing Systems*, 34:19974–19988, 2021. 5
- [10] Wei-Ting Chen, H. Fang, Jian-Jiun Ding, Cheng-Che Tsai, and Sy-Yen Kuo. Jstasr: Joint size and transparency-aware snow removal algorithm based on modified partial convolution and veiling effect removal. In *European Conference on Computer Vision*, 2020. 1
- [11] Wei-Ting Chen, H. Fang, Cheng-Lin Hsieh, Cheng-Che Tsai, I-Hsiang Chen, Jianwei Ding, and Sy-Yen Kuo. All snow removed: Single image desnowing algorithm using hierarchical dual-tree complex wavelet representation and contradict channel loss. *2021 IEEE/CVF International Conference on Computer Vision (ICCV)*, pages 4176–4185, 2021. 1
- [12] Wei-Ting Chen, Zhi-Kai Huang, Cheng-Che Tsai, Hao-Hsiang Yang, Jian-Jiun Ding, and Sy-Yen Kuo. Learning multiple adverse weather removal via two-stage knowledge learning and multi-contrastive regularization: Toward a unified model. In *Proceedings of the IEEE/CVF Conference on Computer Vision and Pattern Recognition*, pages 17653–17662, 2022. 1
- [13] Xiang Chen, Hao Li, Mingqiang Li, and Jinshan Pan. Learning a sparse transformer network for effective image deraining. In *Proceedings of the IEEE/CVF Conference on Computer Vision and Pattern Recognition*, pages 5896–5905, 2023. 2, 5, 1
- [14] Zixuan Chen, Zewei He, and Zhe-Ming Lu. Dea-net: Single image dehazing based on detail-enhanced convolution and content-guided attention. *arXiv preprint arXiv:2301.04805*, 2023. 1
- [15] Shen Cheng, Yuzhi Wang, Haibin Huang, Donghao Liu, Haoqiang Fan, and Shuaicheng Liu. Nbnnet: Noise basis learning for image denoising with subspace projection. In *Proceedings of the IEEE/CVF Conference on Computer Vision and Pattern Recognition*, pages 4896–4906, 2021. 2, 1
- [16] Lu Chi, Borui Jiang, and Yadong Mu. Fast fourier convolution. In *Advances in Neural Information Processing Systems*, 2020. 2
- [17] Sung-Jin Cho, Seo-Won Ji, Jun-Pyo Hong, Seung-Won Jung, and Sung-Jea Ko. Rethinking coarse-to-fine approach in single image deblurring. In *Proceedings of the IEEE/CVF international conference on computer vision*, pages 4641–4650, 2021. 1
- [18] Guy Demoment. Image reconstruction and restoration: Overview of common estimation structures and problems. *IEEE Transactions on Acoustics, Speech, and Signal Processing*, 37(12):2024–2036, 1989. 1
- [19] Yu Dong, Yihao Liu, He Zhang, Shifeng Chen, and Yu Qiao. Fd-gan: Generative adversarial networks with fusion-discriminator for single image dehazing. In *Proceedings of the AAAI Conference on Artificial Intelligence*, pages 10729–10736, 2020. 6
- [20] Qingnan Fan, Dongdong Chen, Lu Yuan, Gang Hua, Nenghai Yu, and Baoquan Chen. A general decoupled learning framework for parameterized image operators. *IEEE Transactions on Pattern Analysis and Machine Intelligence*, 43(1): 33–47, 2019. 6
- [21] Hongyun Gao, Xin Tao, Xiaoyong Shen, and Jiaya Jia. Dynamic scene deblurring with parameter selective sharing and nested skip connections. In *Proceedings of the IEEE/CVF Conference on Computer Vision and Pattern Recognition*, pages 3848–3856, 2019. 6
- [22] Junlin Han, Pengfei Fang, Weihao Li, Jie Hong, Mohammad Ali Armin, Ian Reid, Lars Petersson, and Hongdong Li. You only cut once: Boosting data augmentation with a single cut. In *International Conference on Machine Learning*, pages 8196–8212. PMLR, 2022. 6, 3
- [23] Amir Hertz, Ron Mokady, Jay M. Tenenbaum, Kfir Aberman, Yael Pritch, and Daniel Cohen-Or. Prompt-to-prompt image editing with cross attention control. *ArXiv*, abs/2208.01626, 2022. 4
- [24] Jia-Bin Huang, Abhishek Singh, and Narendra Ahuja. Single image super-resolution from transformed self-exemplars. In *Proceedings of the IEEE Conference on Computer Vision and Pattern Recognition*, pages 5197–5206, 2015. 1, 2

- [25] Jiayi Jiang and Christian Holz. Restore anything pipeline: Segment anything meets image restoration. *arXiv preprint arXiv:2305.13093*, 2023. **3**
- [26] Alexander Kirillov, Eric Mintun, Nikhila Ravi, Hanzi Mao, Chloe Rolland, Laura Gustafson, Tete Xiao, Spencer Whitehead, Alexander C Berg, Wan-Yen Lo, et al. Segment anything. *arXiv preprint arXiv:2304.02643*, 2023. **3**
- [27] Jaakko Lehtinen, Jacob Munkberg, Jon Hasselgren, Samuli Laine, Tero Karras, Miika Aittala, and Timo Aila. Noise2noise: Learning image restoration without clean data. *arXiv preprint arXiv:1803.04189*, 2018. **1**
- [28] Boyi Li, Wenqi Ren, Dengpan Fu, Dacheng Tao, Dan Feng, Wenjun Zeng, and Zhangyang Wang. Benchmarking single-image dehazing and beyond. *IEEE Transactions on Image Processing*, 28(1):492–505, 2018. **5, 1, 2**
- [29] Boyun Li, Xiao Liu, Peng Hu, Zhongqin Wu, Jiancheng Lv, and Xi Peng. All-In-One Image Restoration for Unknown Corruption. In *IEEE Conference on Computer Vision and Pattern Recognition*, New Orleans, LA, 2022. **1, 2, 5, 6, 8**
- [30] Dasong Li, Yi Zhang, Ka Chun Cheung, Xiaogang Wang, Hongwei Qin, and Hongsheng Li. Learning degradation representations for image deblurring. In *European Conference on Computer Vision*, pages 736–753. Springer, 2022. **2, 1**
- [31] Junnan Li, Dongxu Li, Caiming Xiong, and Steven Hoi. Blip: Bootstrapping language-image pre-training for unified vision-language understanding and generation. In *International Conference on Machine Learning*, pages 12888–12900. PMLR, 2022. **4**
- [32] Jingyun Liang, Jiezhong Cao, Guolei Sun, Kai Zhang, Luc Van Gool, and Radu Timofte. Swinir: Image restoration using swin transformer. In *Proceedings of the IEEE/CVF international conference on computer vision*, pages 1833–1844, 2021. **1, 2, 7**
- [33] Xing Liu, Masanori Suganuma, Xiyang Luo, and Takayuki Okatani. Restoring images with unknown degradation factors by recurrent use of a multi-branch network. *arXiv preprint arXiv:1907.04508*, 2019. **3**
- [34] Ilya Loshchilov and Frank Hutter. Sgdr: Stochastic gradient descent with warm restarts. *arXiv preprint arXiv:1608.03983*, 2016. **2**
- [35] Yuning Lu, Jianzhuang Liu, Yonggang Zhang, Yajing Liu, and Xinmei Tian. Prompt distribution learning. In *Proceedings of the IEEE/CVF Conference on Computer Vision and Pattern Recognition*, pages 5206–5215, 2022. **3**
- [36] Ziwei Luo, Fredrik K Gustafsson, Zheng Zhao, Jens Sjölund, and Thomas B Schön. Controlling vision-language models for universal image restoration. *arXiv preprint arXiv:2310.01018*, 2023. **1**
- [37] Jiaqi Ma, Tianheng Cheng, Guoli Wang, Qian Zhang, Xinggang Wang, and Lefei Zhang. Prores: Exploring degradation-aware visual prompt for universal image restoration. *arXiv preprint arXiv:2306.13653*, 2023. **2, 3, 4**
- [38] Kede Ma, Zhengfang Duanmu, Qingbo Wu, Zhou Wang, Hongwei Yong, Hongliang Li, and Lei Zhang. Waterloo exploration database: New challenges for image quality assessment models. *IEEE Transactions on Image Processing*, 26(2):1004–1016, 2016. **5, 1, 2**
- [39] David Martin, Charless Fowlkes, Doron Tal, and Jitendra Malik. A database of human segmented natural images and its application to evaluating segmentation algorithms and measuring ecological statistics. In *Proceedings Eighth IEEE International Conference on Computer Vision. ICCV 2001*, pages 416–423. IEEE, 2001. **1, 2**
- [40] C. McCollough. TU-FG-207A-04: Overview of the low dose CT grand challenge. *Medical Physics*, 43(6):3759–3760, 2016. **4**
- [41] Seungjun Nah, Tae Hyun Kim, and Kyoung Mu Lee. Deep multi-scale convolutional neural network for dynamic scene deblurring. In *Proceedings of the IEEE Conference on Computer Vision and Pattern Recognition*, pages 3883–3891, 2017. **5, 1, 2, 3**
- [42] Srinivasa Narasimhan and Shree Nayar. Vision and the atmosphere. *International Journal of Computer Vision*, 48: 233–254, 2002. **1**
- [43] Dongwon Park, Byung Hyun Lee, and Se Young Chun. All-in-one image restoration for unknown degradations using adaptive discriminative filters for specific degradations. In *2023 IEEE/CVF Conference on Computer Vision and Pattern Recognition*, pages 5815–5824. IEEE, 2023. **1, 2**
- [44] Yanting Pei, Yaping Huang, Qi Zou, Xingyuan Zhang, and Song Wang. Effects of image degradation and degradation removal to cnn-based image classification. *IEEE Transactions on Pattern Analysis and Machine Intelligence*, 43(4): 1239–1253, 2019. **1, 3**
- [45] Vaishnav Potlapalli, Syed Waqas Zamir, Salman Khan, and Fahad Shahbaz Khan. PromptIR: Prompting for all-in-one blind image restoration. *Advances in Neural Information Processing Systems (NeurIPS)*, 2023. **2, 3, 4, 5, 6, 7, 8, 1**
- [46] Alec Radford, Jong Wook Kim, Chris Hallacy, Aditya Ramesh, Gabriel Goh, Sandhini Agarwal, Girish Sastry, Amanda Askell, Pamela Mishkin, Jack Clark, et al. Learning transferable visual models from natural language supervision. In *International conference on machine learning*, pages 8748–8763. PMLR, 2021. **4, 8, 9**
- [47] Robin Rombach, A. Blattmann, Dominik Lorenz, Patrick Esser, and Björn Ommer. High-resolution image synthesis with latent diffusion models. *2022 IEEE/CVF Conference on Computer Vision and Pattern Recognition*, pages 10674–10685, 2021. **3, 4**
- [48] Olaf Ronneberger, Philipp Fischer, and Thomas Brox. U-net: Convolutional networks for biomedical image segmentation. In *International Conference on Medical Image Computing and Computer-Assisted Intervention*, pages 234–241. Springer, 2015. **1**
- [49] Wooksu Shin, Namhyuk Ahn, Jeong-Hyeon Moon, and Kyung-Ah Sohn. Exploiting distortion information for multi-degraded image restoration. In *Proceedings of the IEEE/CVF Conference on Computer Vision and Pattern Recognition*, pages 537–546, 2022. **3**
- [50] Lorenzo Stacchio. Train stable diffusion for inpainting, 2023. **3, 4**
- [51] Xiaole Tang, Xile Zhao, Jun Liu, Jianli Wang, Yuchun Miao, and Tiejong Zeng. Uncertainty-aware unsupervised image deblurring with deep residual prior. In *Proceedings of*

- the *IEEE/CVF Conference on Computer Vision and Pattern Recognition*, pages 9883–9892, 2023. 2, 1
- [52] Chunwei Tian, Yong Xu, and Wangmeng Zuo. Image denoising using deep cnn with batch renormalization. *Neural Networks*, 121:461–473, 2020. 6
- [53] Yuandong Tian and Srinivasa G. Narasimhan. Seeing through water: Image restoration using model-based tracking. *2009 IEEE 12th International Conference on Computer Vision*, pages 2303–2310, 2009. 1
- [54] Zhengzhong Tu, Hossein Talebi, Han Zhang, Feng Yang, Peyman Milanfar, Alan Bovik, and Yinxiao Li. Maxim: Multi-axis mlp for image processing. In *Proceedings of the IEEE/CVF Conference on Computer Vision and Pattern Recognition*, pages 5769–5780, 2022. 2, 1
- [55] Dmitry Ulyanov, Andrea Vedaldi, and Victor Lempitsky. Deep image prior. In *Proceedings of the IEEE Conference on Computer Vision and Pattern Recognition*, pages 9446–9454, 2018. 1
- [56] Ashish Vaswani, Noam M. Shazeer, Niki Parmar, Jakob Uszkoreit, Llion Jones, Aidan N. Gomez, Lukasz Kaiser, and Illia Polosukhin. Attention is all you need. In *Neural Information Processing Systems*, 2017. 4
- [57] Pichao Wang, Xue Wang, Fan Wang, Ming Lin, Shuning Chang, Hao Li, and Rong Jin. Kvt: k-nn attention for boosting vision transformers. In *European conference on computer vision*, pages 285–302. Springer, 2022. 5
- [58] Su Wang, Chitwan Saharia, Ceslee Montgomery, Jordi Pont-Tuset, Shai Noy, Stefano Pellegrini, Yasumasa Onoe, Sarah Laszlo, David J Fleet, Radu Soricut, et al. Imagen editor and editbench: Advancing and evaluating text-guided image inpainting. In *Proceedings of the IEEE/CVF Conference on Computer Vision and Pattern Recognition*, pages 18359–18369, 2023. 3
- [59] Chen Wei, Wenjing Wang, Wenhan Yang, and Jiaying Liu. Deep retinex decomposition for low-light enhancement. *arXiv preprint arXiv:1808.04560*, 2018. 5, 1, 2
- [60] Jason Wei, Xuezhi Wang, Dale Schuurmans, Maarten Bosma, Fei Xia, Ed Chi, Quoc V Le, Denny Zhou, et al. Chain-of-thought prompting elicits reasoning in large language models. *Advances in Neural Information Processing Systems*, 35:24824–24837, 2022. 3, 4
- [61] Yunxuan Wei, Shuhang Gu, Yawei Li, Radu Timofte, Longcun Jin, and Hengjie Song. Unsupervised real-world image super resolution via domain-distance aware training. In *Proceedings of the IEEE/CVF Conference on Computer Vision and Pattern Recognition*, pages 13385–13394, 2021. 2
- [62] Liangbin Xie, Xintao Wang, Chao Dong, Zhongang Qi, and Ying Shan. Finding discriminative filters for specific degradations in blind super-resolution, 2021. 1, 2
- [63] Shaoan Xie, Zhifei Zhang, Zhe Lin, Tobias Hinz, and Kun Zhang. SmartBrush: Text and shape guided object inpainting with diffusion model. In *Proceedings of the IEEE/CVF Conference on Computer Vision and Pattern Recognition*, pages 22428–22437, 2023. 3
- [64] Fuzhi Yang, Huan Yang, Jianlong Fu, Hongtao Lu, and Baining Guo. Learning texture transformer network for image super-resolution. In *Proceedings of the IEEE/CVF Conference on Computer Vision and Pattern Recognition*, pages 5791–5800, 2020. 5, 7, 1, 2
- [65] Wenhan Yang, Robby T. Tan, Jiashi Feng, Jiaying Liu, Zongming Guo, and Shuicheng Yan. Deep joint rain detection and removal from a single image. *2017 IEEE Conference on Computer Vision and Pattern Recognition*, pages 1685–1694, 2016. 1
- [66] Lei Yiming, Li Jingqi, Li Zilong, Cao Yuan, and Shan Hongming. Prompt learning in computer vision: A survey. *Frontiers of Information Technology and Electronic Engineering*, 2023. 3
- [67] Sangdoon Yun, Dongyoon Han, Seong Joon Oh, Sanghyuk Chun, Junsuk Choe, and Youngjoon Yoo. Cutmix: Regularization strategy to train strong classifiers with localizable features. In *Proceedings of the IEEE/CVF international conference on computer vision*, pages 6023–6032, 2019. 6, 3
- [68] Syed Waqas Zamir, Aditya Arora, Salman Khan, Munawar Hayat, Fahad Shahbaz Khan, Ming-Hsuan Yang, and Ling Shao. Multi-stage progressive image restoration. In *Proceedings of the IEEE/CVF Conference on Computer Vision and Pattern Recognition*, pages 14821–14831, 2021. 2, 6, 1
- [69] Syed Waqas Zamir, Aditya Arora, Salman Khan, Munawar Hayat, Fahad Shahbaz Khan, and Ming-Hsuan Yang. Restormer: Efficient transformer for high-resolution image restoration. In *Proceedings of the IEEE/CVF Conference on Computer Vision and Pattern Recognition*, pages 5728–5739, 2022. 1, 2, 5, 6, 7, 8
- [70] Cheng Zhang, Yu Zhu, Qingsen Yan, Jinqiu Sun, and Yan-ning Zhang. All-in-one multi-degradation image restoration network via hierarchical degradation representation. In *Proceedings of the 31st ACM International Conference on Multimedia*, pages 2285–2293, 2023. 5
- [71] Jiale Zhang, Yulun Zhang, Jinjin Gu, Yongbing Zhang, Linghe Kong, and Xin Yuan. Accurate image restoration with attention retractable transformer. *arXiv preprint arXiv:2210.01427*, 2022. 1
- [72] Zhuosheng Zhang, Aston Zhang, Mu Li, Hai Zhao, George Karypis, and Alex Smola. Multimodal chain-of-thought reasoning in language models. *arXiv preprint arXiv:2302.00923*, 2023. 3, 4
- [73] Wang Zhou, Alan Conrad Bovik, Hamid Rahim Sheikh, and Eero P Simoncelli. Image quality assessment: from error visibility to structural similarity. *IEEE Transactions on Image Processing*, 13(4), 2004. 6

Prompt-In-Prompt Learning for Universal Image Restoration

Supplementary Material

Abstract

This supplementary material includes five parts: (A) detailed related work, (B) implementation details, (C) additional results, and (D) discussion.

A. Detailed Related Work

Image restoration. Image restoration aims to recover clean images or signals from their degraded counterparts, which is highly related to the corresponding degradation process. For instance, Gaussian noise, typically seen as noise added to an image, mainly affects high-frequency details. On the other hand, degradations such as rain, snow, and haze are associated with atmospheric light or transmission maps [2, 10, 11, 42, 53, 65], which are multiplied to the clean signal. The blurring or low light degradation can be attributed to blur kernel and global value shift, resulting in distorted structure and color. Because of the intrinsic distinctions among different degradation processes, various models are proposed to tackle individual degradation tasks [7, 14, 15, 30, 32, 51, 54, 68, 69]. Although incorporating prior information of specific degradation into the model design can yield notable performance improvements, this may compromise generalizability across different tasks or even datasets.

Besides task-specific design, most restoration models share similar fundamental designs, such as using transformers to model long-range dependencies [32, 69, 71], employing multi-scale or pyramid architectures with skip connection to leverage features from various layers [17, 68], and spatial attention or gating mechanisms that concentrate on degradation-aware features. Among them, U-Net [48] architectures are particularly popular, which process features at different scales and combine them with skip connections. This helps the network to restore both the structure in deeper layers and the fine details implied by the shadow layers and still demonstrate its superiority in the recent state-of-the-art methods [8, 13, 14, 30, 51, 69].

B. Implementation Details

B.1. Dataset and Preparation

Training and testing datasets. We mainly follow the previous works in data preparation. All the datasets used for training and testing are summarized in Tab. S1. For image denoising, we use a combined set of BSD400 [3] and WED [38] for training and the noisy image are gen-

erated by adding Gaussian noise with different noise levels $\sigma \in \{15, 25, 50\}$. Testing is performed on BSD68 [39] and Urban100 [24]. For single image deraining, we use the Rain100L [64] dataset only, which consists of 200 clean-rainy image pairs for training, and 100 pairs for testing. Regarding image dehazing, we utilize SOTS dataset [28] that contains 72,135 training images and 500 testing images. For image deblurring, we only train the model on GoPro dataset [41] as previous literature [8, 69] with 2103 image pairs for training and 1,111 pairs for testing. For low-light enhancement, we utilize LOL [59] dataset, which contains 485 and 15 pairs for training and testing, respectively.

Data preprocessing. We follow the data preparation procedure in previous works [29, 45]. It is clear that the training data is imbalanced across different tasks, particularly with the dataset of dehazing having significantly more data than others. To tackle this, we adopted the same approach as PromptIR [45], which involves resampling the datasets for other tasks multiple times to match the magnitude of the dehazing data. The resampling ratios are also presented in Tab. S1. All the data are randomly cropped into a size of 128×128 or 200×200 , with random horizontal and vertical flips as data augmentation.

We acknowledge that additional training data, data augmentation, or larger patch sizes can all be beneficial for the training, especially for image deblurring and image dehazing [36, 69]. In this paper, we stick to a normal setting to focus on the effect of the prompt.

B.2. Network and Optimization Details

Details and configuration of PIP. Fig. S1 illustrates the detailed architecture of PIP before prompt-to-prompt interaction. To make sure PIP works independently of the feature map shape, we align the feature map Z with the specific shape of prompts in this phase. Therefore, the prompt dimensions, c for channels, h for height, and w for width, are treated as hyperparameters. The detailed configuration of these hyperparameters for PIP_{Restormer} and PIP_{NAFNet} are presented in Tabs. S2 and S3, respectively. For selective prompt-to-feature interaction, we adopt [13] to set an interval range for top- m selection. This avoids either insufficient information or over-smoothed results. Specifically, we set m at $\frac{C}{2}$, $\frac{2C}{3}$, $\frac{3C}{4}$, and $\frac{4C}{5}$ to create four distinct masks and corresponding outputs, respectively. These outputs are then individually scaled by a single learnable parameter. Finally, we sum these scaled outputs to get the final result of the selective cross-attention.

Detailed configuration of backbone models. We utilize Restormer [69] and NAFNet [8] as the backbone mod-

Table S1. Summary of datasets for various restoration tasks.

Task	Training Set	Test Set	Details	Resampling ratio
Denoising	BSD400 [3], WED [38]	BSD68 [39], URBAN100 [24]	400 and 4744 pairs for training, and 68 and 100 images for testing	$\times 3$
Deraining	Rain100L [64]	Rain100L [64]	200 for training, 100 for testing	$\times 120$
Dehazing	SOTS [28]	SOTS [28]	72135 for training, 500 for testing	$\times 1$
Deblurring	GoPro [41]	GoPro [41]	2103 for training, 1111 for testing	$\times 5$
Enhancement	LOL [59]	LOL [59]	485 for training, 15 for testing	$\times 20$

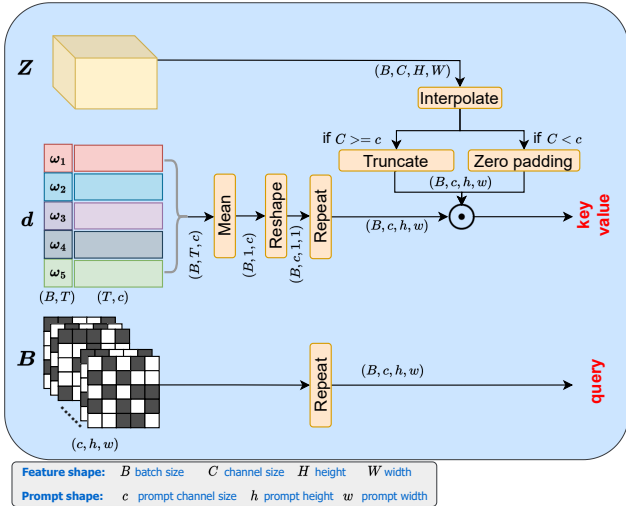


Figure S1. Detailed architecture for generating key, value, and query in our prompt-in-prompt learning.

Table S2. Configuration of hyperparameters for $\text{PIP}_{\text{Restormer}}$. “skip 1” refers to the skip connection in the shadow layer and “skip 3” denotes the deepest ones.

layer	c	$h \times w$
skip 1	64	64×64
skip 2	128	32×32
skip 3	256	16×16

Table S3. Configuration of hyperparameters for $\text{PIP}_{\text{NAFNet}}$. “skip 1” refers to the skip connection in the shadow layer and “skip 4” denotes the deepest ones.

layer	c	$h \times w$
skip 1	64	64×64
skip 2	96	32×32
skip 3	128	16×16
skip 4	128	16×16

els. Restormer is structured as a 4-level U-shape encoder-decoder network with 3 skip connections. We use the default settings of the official implementation, which is available at <https://github.com/swz30/Restormer>. This includes [4, 4, 6, 8] transformer blocks from shal-

low layer to deep layer, respectively. The basic dim of Restormer is 48 as default. PIP is integrated into the three skip connections, with prompt dimensions set to [64, 128, 256] for skip connections, from the shallow layers to deep ones, as presented in Tab. S2. NAFNet is a 5-level U-shape encoder-decoder network with 4 skip connections. We utilize the official code from <https://github.com/megvii-research/NAFNet>, adopting the default architecture designed for image deblurring, which is more balanced in the encoder and decoder. This includes [2, 2, 4, 8] blocks for the encoder, 12 blocks for the middle bottleneck, and [2, 2, 2, 2] blocks for the decoder, respectively. The width of NAFNet is set to 64 as default. Our PIP contains four skip connections, the prompt dim is set to [64, 96, 128, 128] to reduce the computational and memory costs, as shown in Tab. S3.

Training details. PIP is trained alongside the backbone models from scratch for 200 epochs. We employ the cosine annealing schedule with a linear warm-up [34] to control the learning rate. Initially, the learning rate linearly increases to 5×10^{-4} over the first 10 epochs. The learning rate then gradually decreases according to a cosine annealing manner, reaching 0 at the 150-th epoch, and resumes its increase in a cosine manner until the end of the training.

C. Additional Results

C.1. Control by Degradation-aware Models

PIP is designed only to focus on enhancing the restoration performance rather than automatically recognizing different tasks. This is due to the complicated nature of degradation and various requirements in application. For instance, a user may want to remove noise from a low-light image without increasing brightness. However, we argue that controlling PIP with degradation-aware models is applicable and can be easily implemented. For simplicity, we just employ the most commonly used classification backbones, including VGG-16, ResNet-34, and ResNet-34 built with Fourier convolution [16]. We use Fourier convolution based on the observation that some degradations, such as noise and rain, primarily affect high-frequency details, which can be excessively smoothed by spatial convolution. Specifically, we use a ResNet-34 built with fast Fourier

convolution from the official implementation at <https://github.com/pkumivision/FFC>.

All three classification backbones are trained on a task to classify the five different types of degradation. The training is conducted on 4 RTX4090 GPUs, with a batch size of 128 and an initial learning rate of 0.01. The Adam optimizer is employed with $\beta_1 = 0.9$ and $\beta_2 = 0.999$, respectively. The learning rate is reduced by half every 30 epochs. We maintain consistent data preparation and train the model for a total of 200 epochs.

Table S4. Accuracy of degradation-aware models in degradation classification.

Task	VGG16	ResNet-34	ResNet-34 w/ Fourier
Noise	0.00	98.04	100.00
Rain	0.00	99.00	100.00
Haze	100.00	95.60	100.00
Blur	0.00	100.00	100.00
Low light	0.00	100.00	100.00

Tab. S4 presents the results. Unsurprisingly, we find that a simple degradation-aware model built with fast Fourier convolution can easily obtain 100% accuracy on all five tasks, demonstrating that it can *easily control PIP without a performance drop*. We also observe that ResNet-34 also achieves a good performance while VGG-16 collapses in the training. The reason is that VGG contains a series of downsampling layers without enough skip connections to preserve the low-level details. In comparison, ResNet can better fit the task of degradation classification.

C.2. Training with Multiple Prompts

In real-world scenarios, a key challenge is that images can suffer from multiple types of degradation simultaneously. Existing datasets seldom contain such cases. To investigate the capability of tackling multiple degradations, one straightforward strategy is to simulate various degradations on a clean image [41, 44]. However, accurately replicating real-world conditions remains challenging, especially for degradation like haze and blur. This also presents a significant challenge for restoration models, as they must adapt to a wide range of degradation combinations and permutations [33, 49].

Despite the challenges of the task, we explore the potential of training the restoration model using multiple prompts with data augmentation. Inspired by augmentation techniques that blend multiple images into one [67], or apply various enhancements to a single image [22], and can improve the classification performance, we design an augmentation strategy for training called Degradation-Mix (DMIX), as shown in Fig. S2. Similar to Cut-Mix [22], we first split all images in a mini-batch into two halves, either horizontally or vertically. These halves are then randomly

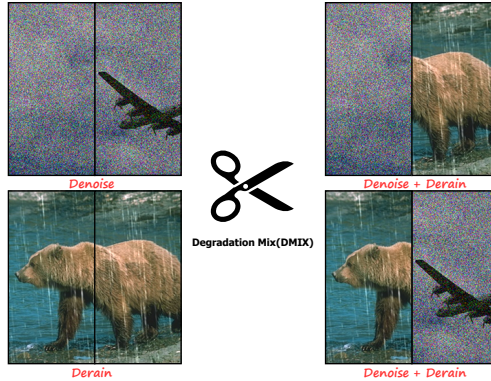


Figure S2. Illustration of Degradation-Mix data augmentation in the horizontal axis.

Table S5. Result of PIP trained with multiple prompts. Metrics are presented in [PSNR (dB) / SSIM].

Method	Rain100L + Noise	Haze + Noise
PIP _{Restormer}	26.50/0.771	16.58/0.754
PIP _{Restormer} w/ DMIX	26.79/0.815	20.61/0.741

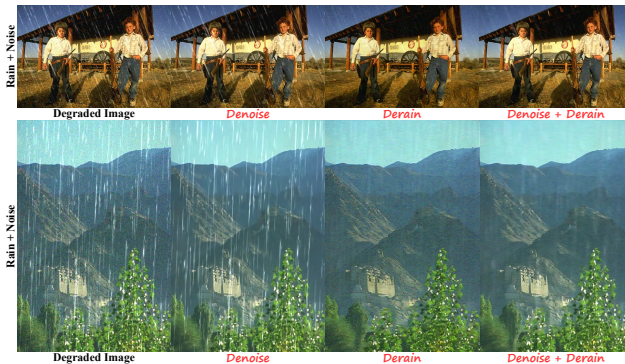


Figure S3. Visualization of PIP restoration with different prompts.

shuffled to create new images with combined degradations. Concurrently, we mix the corresponding degradation labels to align with the degradation-aware prompt. By training PIP with DMIX, we observe that PIP exhibits improved generalization in handling images with mixed degradations, as seen in Tab. S5. We also find that it produces better visual results by using multiple prompts at the same time, as shown in Fig. S3. However, we also observe some remaining artifacts and the quality of the restored image was not optimal. These results underline the flexibility and potential of the proposed prompt-in-prompt learning. Future research could focus on utilizing multiple prompts collaboratively addressing mixed degradations.

Table S6. Generalization to real-world denoising and medical image denoising. Metrics are presented in [PSNR (dB) / SSIM].

Dataset	AirNet	PromptIR	PIP _{Restormer}
SIDD [1]	23.66/0.356	24.32/0.378	24.12/0.362
AAPM [40]	34.59/0.936	34.61/0.9432	34.67/0.919

C.3. Generalization on Real-World Data

The results in Tab. S6 reveal that all three methods struggle with zero-shot performance on unseen types of degradation, such as noise in the SIDD [1] dataset that consists of real camera noise rather than Gaussian noise. When generalizing to medical images in “2016 NIH-AAPM-Mayo Clinic Low-Dose CT Grand Challenge” (AAPM) dataset [40] affected by Gaussian noise with $\sigma = 25$, all three methods perform relatively better.

Although PIP performs relatively better than compared methods in these scenarios, we found that the generalizability is still *mainly determined by the backbone model*. Conventional restoration backbones are less effective with new degradation types, despite being efficient in inference. On the other hand, popular diffusion-based methods show better adaptability across various tasks [47, 50] while requiring more time for inference and higher computational costs. Choosing an appropriate backbone model involves a trade-off. Hence, the challenge of adapting a trained model to new types of degradation remains an open question and could be a promising direction for future research.

C.4. More Visual Results

Figs. S4, S5, and S6 show more visualization results of PIP and other universal restoration methods. Generally, we find that PIP achieves optimal visual effect.

D. More Discussion

In summary, the proposed prompt-in-prompt learning effectively enhances existing backbones in universal image restoration and surpasses recent methods with only a slight increase of computational cost. Prompt-in-prompt learning merges the advantages of high-level degradation-aware prompt and low-level basic restoration prompt, thereby offering clear interpretability and flexible control options, whether through human intervention or degradation-aware models. We emphasize that both PIP and designed modules can be easily adapted to other backbone models and tasks in low-level vision.

Limitations. First, PIP still introduces some computational costs in both training and inference phases, although these are substantially lower than those of comparative methods. Second, we observe that PIP does not significantly enhance the generalization capabilities of models to unknown degradations. Although this may be attributed to

the backbone models and limited parameters, it is worth investigating whether prompt-in-prompt learning can be beneficial for large-scale restoration models. Furthermore, exploring how to use prompts to boost the zero-shot performance of restoration models is also a worthwhile field.



Figure S4. Visual comparison of universal methods on image denoising with a Gaussian noise level $\sigma = 15, 25, 50$, from the first to the third row, respectively.

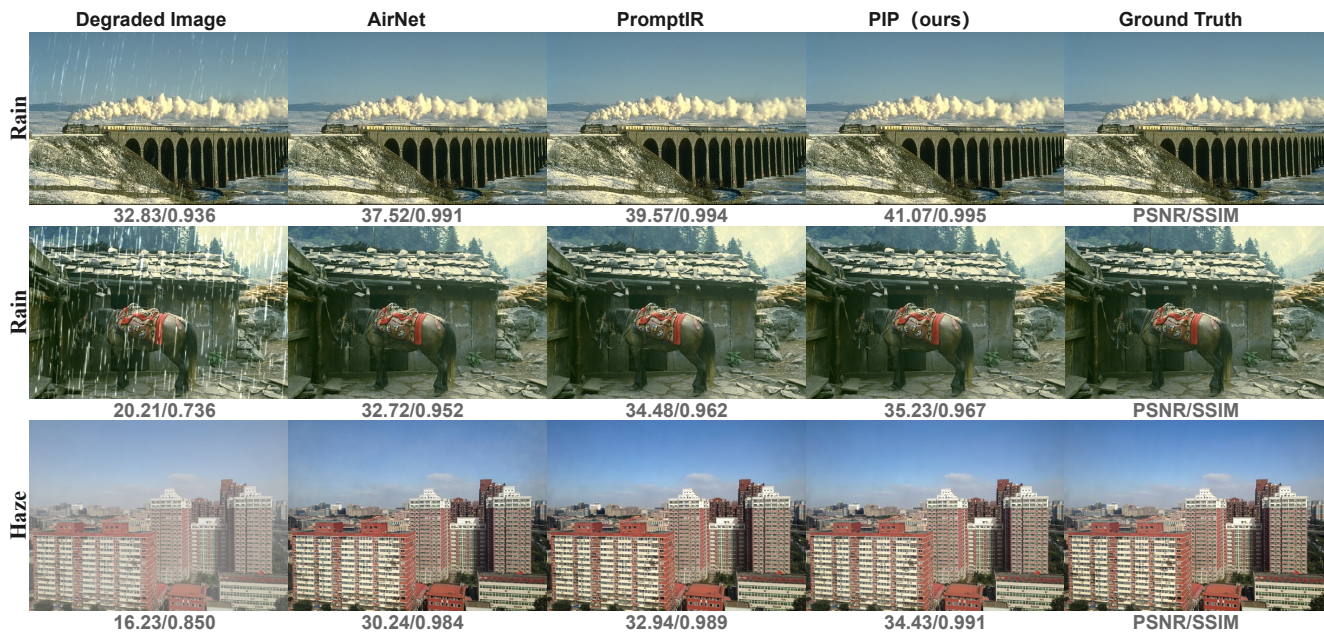


Figure S5. Visual comparison of universal methods on image deraining and dehazing.

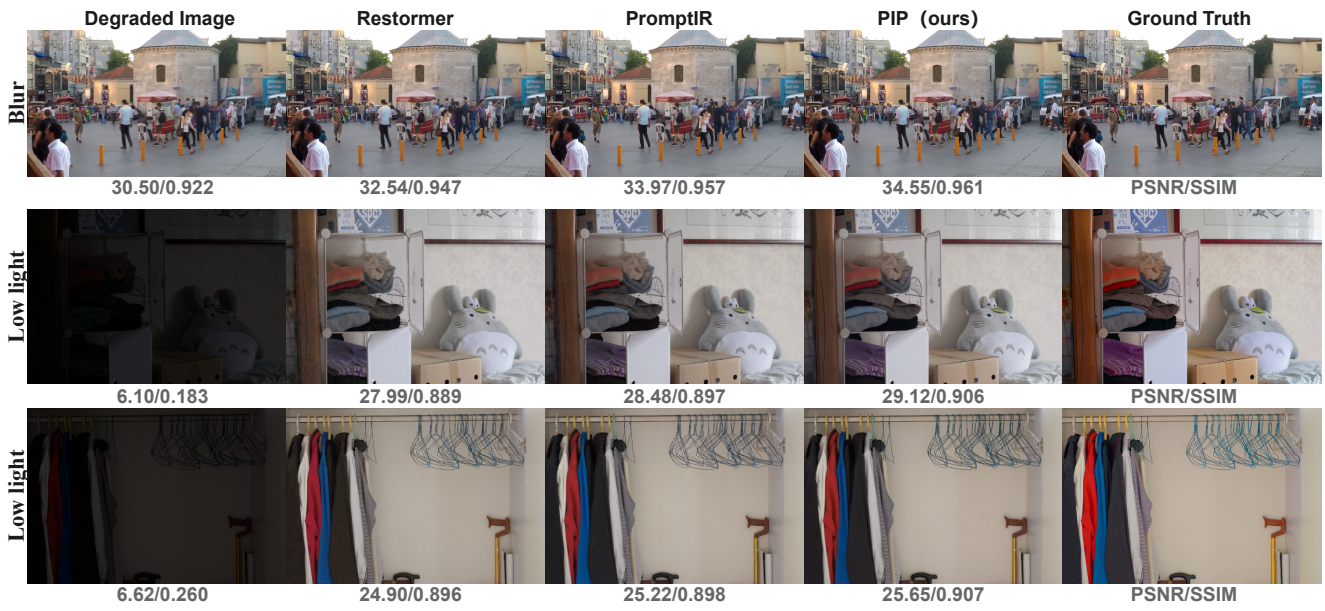


Figure S6. Visual comparison of universal methods on image deblurring and low light enhancement.